

MICROSCOPIC CALCULATION
OF CHARGE BALANCE FUNCTIONS

By

Vinzent Steinberg

A THESIS

Submitted to
Michigan State University
in partial fulfillment of the requirements
for the degree of

Physics—Master of Science

2015

ABSTRACT

MICROSCOPIC CALCULATION OF CHARGE BALANCE FUNCTIONS

By

Vinzent Steinberg

Charge balance functions have been proposed to study the quark-gluon plasma hypothesized to form in relativistic heavy-ion collisions [1]. Motivated by previous work [2], a microscopic model is developed that considers the evolution of thermal quark-antiquark pairs in the quark-gluon plasma to calculate hadronic balance functions based on the chemical properties of the plasma. This involves modeling the generation of the quarks given the hydrodynamic properties of the quark-gluon plasma combined with what we know about its chemistry from lattice quantum chromodynamics, as well as modeling the separation of these quarks and their hadronization. After feeding the resulting hadrons into a cascade where they scatter and decay, the balance function for any combination of hadrons species can be calculated.

ACKNOWLEDGEMENTS

I would like to thank all the people who contributed in some way to the work in this thesis. First and foremost, I thank my advisor, Professor Scott Pratt, who taught me how to think like a theorist. His help and support have been outstanding, especially during the final stages of this thesis. His contributions to the work presented here are indispensable. I would also like to thank my committee members Professor Carl Schmidt and Professor Gary Westfall for their interest in my work. A special thanks goes out to Debbie Barratt who was of great help whenever I had administrative problems. I am grateful for the discussions, insight and friendship my fellow grad students shared with me. They shaped my experience at MSU.

I would like to thank my family for their unyielding support in everything I do.

I am grateful for the financial support provided by Michigan State University and the German National Academic Foundation.

TABLE OF CONTENTS

LIST OF FIGURES	vi
Chapter 1 Introduction	1
Chapter 2 Theory	5
2.1 Required Concepts	6
2.1.1 Bjorken Coordinates	6
2.1.2 Modeling Heavy-Ion Collisions	8
2.1.2.1 Canonical Picture	8
2.1.2.2 Hypersurface Element	8
2.2 Generating Quarks	9
2.2.1 Charge Correlation	9
2.2.2 Quark Pair Production Rate	12
2.3 Separating Quarks	13
2.3.1 Random Walk	14
2.3.2 Causal Diffusion Equation	15
2.3.3 Modeling Relativistic Diffusion	16
2.3.3.1 Derivation of a Relativistic Propagator	16
2.3.3.2 Comparison of Propagators	18
2.3.3.3 Random Walk vs. Propagator	18
2.4 Generating Hadrons	18
2.4.1 Hadron Production Rate	18
2.4.2 Maxwell-Jüttner Distribution	23
2.4.3 Hadron Production Rate – Continued	25
2.4.3.1 Non-Relativistic Limit	26
2.4.3.2 Ultra-Relativistic Limit	27
Chapter 3 Implementation	28
3.1 Generation of Quark Pairs	28
3.2 Diffusion of Quarks	30
3.3 Hadronization	33
3.4 Hadron Cascade	37
3.5 Calculating Balance Functions	37
3.5.1 Contribution above Freezeout Temperature	38
3.5.2 Contribution below Freezeout Temperature	38
Chapter 4 Conclusion	40
4.1 Summary	40
4.2 Future Work	41
APPENDICES	43

Appendix A: Notation and Conventions	44
Appendix B: Normalization of Maxwell-Jüttner Distribution	46
BIBLIOGRAPHY	47

LIST OF FIGURES

Figure 1.1	Diagram summarizing the proposed model to calculate the charge balance function.	4
Figure 2.1	Plot of the diffusion propagators as functions of position x and time t for different space and time step sizes Δx and Δt . The continuous lines show the classical Wiener propagator, the dashed lines the generalized relativistic one. The dots show the corresponding binomial probabilities to diffuse from position 0 to x given a random walk. To guide the eye, the dots are connected by dotted lines. Note that the dots have to be compared to the area under the corresponding segment of the continuous propagators. As expected, for smaller Δx the propagators are narrower. Also, the difference between the relativistic and the non-relativistic propagator becomes smaller with decreasing Δx . This is to be anticipated, because the diffusion speed $\Delta x/\Delta t = 0.5$ is smaller than before ($\Delta x/\Delta t = 1$).	19
Figure 2.2	Plot of probability p to end up at position x after a one-dimensional random walk. The blue line is a histogram for x after the specified amount of steps. The green line is the classical propagator integrated in time, the red line the relativistic one integrated in time. While the relativistic propagator is narrower and actually vanishes at the maximal possible x , the results are very similar. For a high amount of random steps, the random walk histogram is very close to the propagators.	20
Figure 3.1	Charge fluctuation χ over entropy s as a function of temperature T for various quark pairs. The dotted vertical line represents the freezeout temperature at 165 MeV. The solid lines represent the results of lattice QCD simulations of a quark-gluon plasma [32]. The dashed lines show the results of assuming a hadron gas in thermal equilibrium (2.13). Note that for high temperatures χ/s is roughly constant according to lattice QCD, and the offdiagonal element (χ_{us}) vanishes as expected for the parton gas model (2.14). The hadron gas model roughly agrees with the lattice data for small temperatures. For high temperatures it does not, in that limit we expect the plasma to behave like a parton gas where all light species are the same, because their masses are significantly smaller than the temperature ($m_u \approx m_d \ll m_s \approx 100$ MeV). This expectation is confirmed by the lattice data.	31
Figure 3.2	Temperature T as a function of space (x, y) in the transverse plane. The solid line represents the freezeout temperature at 165 MeV. This was taken at the beginning of an Israel-Stewart hydrodynamics simulation (see [33] for the implementation).	32

Figure 3.3	Example of a random walk as implemented here. This shows the diffusion trajectories of a random sample of quarks from the first population until they freeze out. The trajectories are projected to the transverse plane.	34
Figure 3.4	An illustration of the modified Bresenham algorithm used. Each square cut by the diffusion trajectory has to be considered, because it is a possibility for a freezeout.	35

Chapter 1

Introduction

The quark-gluon plasma is a phase consisting of partons that is believed to form at high temperatures and densities, comparable to the first few microseconds after the Big Bang. In relativistic heavy-ion collisions at RHIC (Relativistic Heavy Ion Collider) and at the LHC (Large Hadron Collider) matter is created with energy densities near $10 \text{ GeV}/\text{fm}^3$. This is above the threshold for defining individual hadrons. The chemistry of an equilibrated quark-gluon plasma is well understood: There are 3 light quark species and 8 gluons with a total of 52 degrees of freedom. Such a plasma can be modeled using lattice quantum chromodynamics. However, there has been little experimental evidence that the matter created in heavy-ion collisions has chemical properties close to those of equilibrated matter. It is not possible to measure the quarks in the plasma directly, which makes it challenging to infer the chemistry of the partonic matter.

A promising approach at looking through this haze of hadronization are *charge balance functions*. They measure the pairwise correlations between charges as a function of relative rapidity. The correlations are driven by the local charge conservation in heavy-ion collisions. Hadrons are produced in pairs of opposite charge that are separated in rapidity due to thermal motion and diffusion into regions of different collective velocity. If their creation is delayed they will have less time to separate, yielding a contribution to the

balance function for small relative rapidities, whereas hadrons created early contribute for larger relative rapidities.

Balance functions have first been suggested for investigating hadronization in jets produced by proton-proton [3, 4] and electron-positron [5] collisions. Later it was proposed to use them for testing the quark-gluon plasma hypothesis [1], in particular for understanding when the quarks are created and how they are diffused. The existence of a quark-gluon plasma implies delayed hadronization, which would make the balance functions narrower for the reasons discussed above.

The STAR collaboration measured balance functions for gold-gold, deuteron-gold and proton-proton collisions at RHIC [6–10]. They are defined for each event as

$$B_{\alpha\bar{\alpha}}(\Delta y) = \frac{1}{2} \left(\frac{N_{\alpha\bar{\alpha}}(\Delta y) - N_{\alpha\alpha}(\Delta y)}{N_{\alpha}} + \frac{N_{\bar{\alpha}\alpha}(\Delta y) - N_{\bar{\alpha}\bar{\alpha}}(\Delta y)}{N_{\bar{\alpha}}} \right) \quad (1.1)$$

where α is a hadron species and $\bar{\alpha}$ the corresponding anti-species (for example π^+ and π^-). $N_{\alpha\beta}$ is the number of $\alpha\beta$ pairs separated in rapidity by Δy . N_{α} is the total number of α particles. For central collisions the balance functions were narrower, as expected if there is a quark-gluon plasma. Only for high impact parameters was the width in agreement with models based on independent nuclear scattering [11, 12]. This confirmed the predictions made in [1]. Additionally, the experimental results have been compared with a microscopic hadronic model and a blast-wave model, where only the latter could correctly describe the spectra [13].

Similarly, balance functions have been measured for proton-proton, carbon-carbon and lead-lead collisions at CERN SPS [14]. It was shown that the width of the balance function decreased with increasing centrality and nucleus size, again confirming the predictions stemming from the assumption of delayed hadronization due to the existence of a quark-gluon plasma.

The small width of the balance function can also be explained with a coalescence

rehadronization model [15]. Furthermore, pion balance functions have been calculated in good agreement with the STAR data using a thermal model that considers decays [16].

Balance functions can be binned by the azimuthal separation $\Delta\phi$. This has been proposed to constrain the amount of transverse flow at freezeout [17, 18] and can be calculated from two-particle angular correlations measured at RHIC [19].

The models discussed so far did not consider balance functions for different species. The first one that did assumed the existence of two charge creation waves: one when the quark-gluon plasma forms and one when it hadronizes [2]. For a chemically equilibrated quark-gluon plasma one would expect that most of the electric charge is created in the second wave, while most of the strangeness is created in the first one. Because pions carry most of the charge and kaons most of the strangeness, this implies that the K^+K^- balance function is broader than the $\pi^+\pi^-$ balance function. For protons the balance function should be dominated by baryon conservation. Because of the drop of baryon susceptibility at hadronization, the second wave contributes negatively to the $p\bar{p}$ balance function, resulting in a dip at small relative rapidity. Fitting the model to preliminary STAR results [10] showed that the data exposes a chemical makeup that agrees within a 20% error margin with results from lattice simulations of a quark-gluon plasma. By considering all three balance functions, it was made clear that assuming the creation of charge at one time is inconsistent with the data.

The goal of this thesis is to develop a model in the spirit of [2] that uses a microscopic simulation of the quark pairs instead of the simple parametric model assuming two charge creation waves. This should be more accurate, since quark pairs are continuously produced during the evolution of the reaction. Such a model could improve our understanding of the microscopic properties of the quark-gluon plasma, for example it might be possible to determine its diffusion constant.

The canonical picture of a relativistic heavy-ion collision is the following: During the collision a quark-gluon plasma is formed that can be described as a hydrodynamic region.

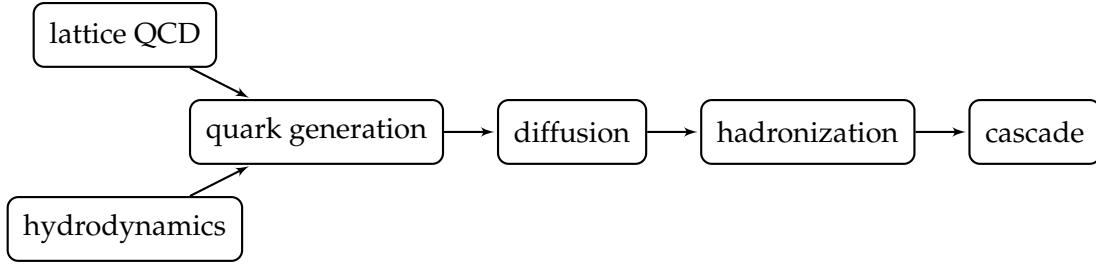


Figure 1.1 Diagram summarizing the proposed model to calculate the charge balance function.

The plasma evolves and cools down, until it is cold enough for hadronization to take place (at ca. 165 MeV). The resulting hadrons scatter and decay in a cascade before they can be observed in a detector. In this picture the proposed model can be roughly divided into the following steps:

1. Generate up, down and strange charges in the hydrodynamic phase.
2. Model the separation of the charges by diffusion.
3. Translate the charges into hadrons at the interface of the hydrodynamic region and the cascade.
4. Scatter and decay hadrons.

After performing those steps, the balance functions can be directly calculated from the hadrons. This thesis tries to address step 1, 2 and 3, for which the theory is discussed in chapter 2. The implementation details of the model and how everything fits together is explained in chapter 3.

Chapter 2

Theory

There are two contributions to the balance function that have to be considered:

1. The contribution due to the quark pairs generated *above the freezeout temperature* that freeze out to correlated hadrons.
2. The contribution due to uncorrelated hadrons *below the freezeout temperature* that decay and annihilate each other while being spread in space by collisions.

Modeling the first contribution is the topic of this chapter. For the second contribution an existing cascade code can be used [20], which will be discussed in more detail in chapter 3.

This chapter provides the background and theoretical description of a method for generating and propagating correlated quark-antiquark pairs during the evolution of the heavy-ion collision. We then show how those correlated quarks can be projected onto correlated hadrons, and ultimately into measurable correlations of the final state.

In the first section a very convenient set of coordinates is introduced, which are used for defining the balance functions. They also give some insight into the hydrodynamic evolution of the plasma.

The quark pairs contribute to the balance functions in three steps:

1. The pairs are generated according to thermal equilibrium (section 2.2).

2. The pairs separate in a diffusive process (section 2.3).
3. The individual quarks hit the freezeout surface and hadronize (section 2.4).

This yields hadrons that can be correlated by tracing back the original quark pairs, enabling the calculation of balance functions.

2.1 Required Concepts

2.1.1 Bjorken Coordinates

In highly relativistic heavy-ion collisions it can be observed that in the center-of-momentum frame small boosts should not influence the observables, because the colliding nucleons are at much larger rapidities than the thermal velocities of the created particles [21]. In such a boost-invariant system the flow is not accelerated in the longitudinal direction, because there are no gradients able to cause an acceleration. This means that the longitudinal component of the velocity of a hydrodynamic fluid element is approximately constant.

Motivated by these considerations, we define the *proper time* τ and the *spatial rapidity* η :

$$\tau := \sqrt{t^2 - z^2} \qquad \eta := \tanh^{-1} \left(\frac{z}{t} \right) \qquad (2.1)$$

$$\Leftrightarrow \quad z = \tau \sinh \eta \qquad t = \tau \cosh \eta \qquad (2.2)$$

Under boosts in z -direction the proper time τ is invariant and the rapidity η is shifted by a constant. As we will see later in this section, local quantities depend only on τ and are independent of η .

For small η and small z , Equation 2.2 can be approximated by

$$\tau = t \qquad \eta = \frac{z}{t} \qquad (2.3)$$

$$\Leftrightarrow \quad z = \tau \eta \qquad t = \tau . \qquad (2.4)$$

This corresponds to the ultrarelativistic limit, where z will be small due to the Lorentz contraction.

The hydrodynamic equation for the entropy density s is given by the continuity equation:

$$0 = \partial_\mu (su^\mu) = s\partial_\mu u^\mu + u^\mu \partial_\mu s, \quad (2.5)$$

where \mathbf{u} is the 4-velocity of the fluid. This can be rewritten in Bjorken coordinates using that τ is the time in the rest frame and that $u_z = \frac{z}{\tau}$ (no acceleration):

$$u_\mu \partial^\mu = \partial_\tau \quad \partial^\mu u_\mu = \frac{1}{\tau}, \quad (2.6)$$

resulting in a much simpler equation for the entropy:

$$0 = \frac{s}{\tau} + \partial_\tau s \quad (2.7)$$

This yields a solution that does not depend on η :

$$s(\tau) = s(\tau_0) \frac{\tau_0}{\tau} \quad (2.8)$$

If we assume a non-interacting gas of massless partons, then the density of each parton species scales with the entropy. In an isentropic expansion of this gas the number of each species must thus be conserved until hadronization.

By assuming an equation of state relating the energy density ϵ and the pressure p (for instance $p = \epsilon/3$ for an ideal gas of massless partons), it can be shown that the temperature and energy density similarly only depend on τ .

2.1.2 Modeling Heavy-Ion Collisions

2.1.2.1 Canonical Picture

When simulating relativistic heavy ion collisions, it is appropriate to model the quark-gluon plasma using hydrodynamics as long as the collisions are sufficiently rapid so that all the species move with a single collective velocity and a single local kinetic temperature. At some point of the reaction (or far away enough from the center) the plasma is cold enough that those conditions are no longer met. The hadrons will then move independently, and a microscopic model based on binary interactions should take over. Those models are usually called "hadronic cascades". For many particles (or high oversampling) they approach a Boltzmann description [22].

2.1.2.2 Hypersurface Element

The decoupling temperature defines a surface separating the hydrodynamic description and the cascade interface. At this surface hadrons are emitted from the hydrodynamic region into the cascade.

We define a hypersurface A using a scalar function C of the 4-vector¹ \mathbf{x} :

$$A := \{\mathbf{x} \in \mathbb{R}^4 \mid C(\mathbf{x}) = 0\} \quad (2.9)$$

The hypersurface is described by local quantities, usually the temperature or density, e.g. $C(\mathbf{x}) = T(\mathbf{x}) - T_0$. If C is positive inside the hydrodynamic region and negative outside of it, then the corresponding *hypersurface element* per 4-volume is

$$\Omega^\mu(\mathbf{x}) = -\partial^\mu \theta(C(\mathbf{x})) = -\delta(C(\mathbf{x})) \partial^\mu C(\mathbf{x}) . \quad (2.10)$$

Ω is orthogonal to the surface. Multiplying C by a positive constant does not change Ω_μ .

¹ The following notation will be used in this document: 4-vectors are typeset in bold (\mathbf{x}), 3-vectors have an arrow on top (\vec{x}) and vector components use the normal font style (t, x, y, z).

For $C(\mathbf{x}) = T(\mathbf{x}) - T_0$ this definition implies that Ω_μ is parallel to $-\partial_\mu T$.

Given a 4-momentum distribution $f(\mathbf{p})$ at the boundary, the number of particles emitted through a hypersurface element Ω is given by the Cooper-Frye formula [23]:

$$dN = \int d^4x \frac{\Omega(\mathbf{x}) \cdot \mathbf{p}}{E_p} f(\mathbf{p}) \frac{d^3p}{(2\pi)^3} \quad (2.11)$$

We will need this later to calculate how many hadrons are to be generated during freeze-out.

2.2 Generating Quarks

In this section a formula for the source function of thermal quark pairs is derived. These correlated pairs will ultimately be used to generate the charge balance correlations seen in experiment. For this, it is helpful to introduce charge fluctuation for quarks which can be related to the charge correlations of hadrons. The source function enables us to generate quark pairs in the quark-gluon plasma given its hydrodynamic evolution.

2.2.1 Charge Correlation

Consider the correlation of two quark charges a, b separated by the spatial rapidity η . Here we only care about up, down and strange quarks, since the other quarks are too heavy to exist in significant quantities. Then their *charge fluctuation* is given for a box of volume V by

$$\chi_{ab} := \frac{\langle Q_a Q_b \rangle - \langle Q_a \rangle \langle Q_b \rangle}{V} \quad (2.12)$$

For zero net charge, the last term vanishes. This is a reasonable assumption for many measurements of heavy-ion collisions at LHC or at the highest RHIC energies.

For a non-interacting hadron gas we can assume that only quarks confined to the same

hadron are correlated, yielding

$$\chi_{ab} = \sum_{\alpha} \langle n_{\alpha} \rangle q_{\alpha,a} q_{\alpha,b} , \quad (2.13)$$

where the sum goes over all hadron species α and n_{α} is the hadron number density.

For a non-interacting parton gas, the quarks are only correlated with themselves. Assuming unit charge, we get

$$\chi_{ab} = \delta_{ab} \left(\langle n_a \rangle + \langle n_{\bar{a}} \rangle \right) . \quad (2.14)$$

The *charge correlation* for a given difference in spatial rapidity η is

$$g_{ab}(\eta) := \langle \rho_a(0) \rho_b(\eta) \rangle - \langle \rho_a(0) \rangle \langle \rho_b(\eta) \rangle \quad (2.15)$$

where ρ_a is the density of a charges. That is, the difference of the number density of a quarks and the number density of \bar{a} quarks.

If the net charge is zero, the last term vanishes as before. χ_{ab} corresponds to the charge correlation at $\eta = 0$:

$$\chi_{ab} = \int_0^{\epsilon} g_{ab} \, d\eta \quad \text{for small } \epsilon . \quad (2.16)$$

For an equilibrated system χ_{ab} can be taken from calculations based on the grand canonical ensemble, such as lattice gauge theory.

If the local correlation is equilibrated and if the spatial extent of the correlation is smaller, the charge flux can be expressed in terms of the correlation. Since the net charge is zero

$$\int_0^{\infty} g_{ab} \, d\eta = 0 , \quad (2.17)$$

this implies

$$\int_{\epsilon}^{\infty} g_{ab} \, d\eta = -\chi_{ab} . \quad (2.18)$$

Since ρ_α refers to the density of a conserved charge, it may be predicted by a model, i.e. quantumchromodynamical simulations on a lattice. This will be discussed in more depth in section 3.1.

Once we know g_{ab} , we need to understand how this translates into a correlation between hadrons. We quantify this correlation between hadron species α, β separated by spatial rapidity η :

$$G_{\alpha\beta}(\eta) := \left\langle (n_\alpha(0) - n_{\bar{\alpha}}(0))(n_\beta(\eta) - n_{\bar{\beta}}(\eta)) \right\rangle \quad (2.19)$$

This is directly related to the quark charge correlation:

$$g_{ab}(\eta) = \sum_{\alpha\beta} G_{\alpha\beta}(\eta) q_{\alpha,a} q_{\beta,b} \quad (2.20)$$

where $q_{\alpha,a}$ is the a -charge of hadron species α . As shown by Pratt [24], for vanishing net charge we can relate $G_{\alpha\beta}$ to the properties of the quarks:

$$G_{\alpha\beta}(\eta) = 4 \sum_{abcd} \langle n_\alpha \rangle q_{\alpha,a} \chi_{ab}^{-1}(0) g_{bc}(\eta) \langle n_\beta \rangle q_{\beta,d} \chi_{cd}^{-1}(\eta) \quad (2.21)$$

This equation links the measurable charge correlations of the hadrons with the properties of the quark-gluon plasma, which cannot be directly observed.

The *charge balance function* can be calculated from the correlation function by dividing by the multiplicity:

$$B_{\alpha\beta}(\eta) = \frac{G_{\alpha\beta}(\eta)}{\langle n_\beta \rangle + \langle n_{\bar{\beta}} \rangle} \quad (2.22)$$

where $\langle n_\beta \rangle$ is the number of β hadrons per unit rapidity. It represents the additional density of seeing an $\alpha - \bar{\alpha}$ given one observed an extra $\beta - \bar{\beta}$. Note that the normalization is slightly different from the one used for the experimentally measured balance function (1.1). However, for vanishing net charge we often have $\langle n_\alpha \rangle \approx \langle n_{\bar{\alpha}} \rangle$, which makes the two

definitions (2.22) and (1.1) identical.

Balance functions have been measured for various species [6–10, 14, 19].

2.2.2 Quark Pair Production Rate

In the previous section it was shown how g_{ab} could be used to calculate correlations between hadrons. To calculate g_{ab} , we need to model the creation of balancing charges and their separation. In this section we derive a formula for the pair production rate. We will assume that we are given the hydrodynamic evolution of the quark-gluon plasma. That is, we know the solution to the hydrodynamic equations, in particular: the entropy density s , the particle number density n and the fluid 4-velocity \mathbf{u} as functions of the 4-position \mathbf{x} .

Those solutions depend on the initial conditions of the hydrodynamic problem, which are essentially the parameters of the heavy-ion collision, such as beam energy, centrality or the type of the colliding nuclei.

For sources σ and ν , continuity demands for the entropy current s

$$\partial_\mu(su^\mu) = \sigma \quad \Leftrightarrow \quad u^\mu \frac{\partial_\mu s}{s} = \frac{\sigma}{s} - \partial_\mu u^\mu \quad (2.23)$$

and the particle current n :

$$\partial_\mu(nu^\mu) = \nu \quad \Leftrightarrow \quad u^\mu \frac{\partial_\mu n}{n} = \frac{\nu}{n} - \partial_\mu u^\mu \quad (2.24)$$

Combining (2.23) and (2.24) gives

$$u^\mu \partial_\mu \frac{n}{s} = \frac{n}{s} \left(\frac{u^\mu \partial_\mu n}{n} - \frac{u^\mu \partial_\mu s}{s} \right) = \frac{n}{s} \left(\frac{\nu}{n} - \frac{\sigma}{s} \right). \quad (2.25)$$

Assuming there is a particle source ($v \neq 0$), but entropy is conserved ($\sigma = 0$), this gives

$$su^\mu \partial_\mu \frac{n}{s} = v . \quad (2.26)$$

Identifying n with $-\chi_{ab}$, we obtain the number of correlated quark pairs

$$dN_{ab} = v d^4x = -su^\mu \partial_\mu \left(\frac{\chi_{ab}}{s} \right) d^4x . \quad (2.27)$$

In the fluid rest frame this simplifies to

$$dN_{ab} = -s \partial_t \left(\frac{\chi_{ab}}{s} \right) d^4x . \quad (2.28)$$

This means that there are no pairs created if the charge fluctuation per entropy is constant in time.

The ratio $\frac{\chi_{ab}}{s}$ as a function of temperature T can be obtained from the results of lattice quantum chromodynamics calculations or by assuming a thermalized hadron gas. The temperature as a function of spacetime is given by the hydrodynamical model. Combining both, we can calculate the rate of pair generation for each hydro cell. All this will be discussed in more detail in chapter 3.

2.3 Separating Quarks

In the previous section we derived which quark pairs should be generated where. Each pair is created at one point in spacetime and the two partner quarks are correlated. Since their separation is zero, this implies a contribution to the two-particle correlation function corresponding to the type of the pair at $\eta = 0$. However, due to their considerable thermal energy, the two quarks will move apart, yielding contributions at $\eta \neq 0$.

We will model this separation as a diffusive process. Similarly to the hydrodynamic

model of the quark-gluon plasma, this approach is only valid if the particles are dense enough to collide with each other multiple times. Their mean free path should be smaller than the size of the fireball. The aim of this section is to find a way to diffuse the generated thermal quarks that is consistent with relativity.

The first subsection shows how a random walk and the non-relativistic diffusion equation are related. This gives a way to express the diffusion constant in terms of the random walk parameters. In the second subsection, a simple causal generalization of the diffusion equation is derived. However, this approach has some issues which are discussed. The last subsection compares an approach remedying those issues (as suggested in [25]) to a very simple relativistic random walk. This serves as a verification that the random walk is a valid approach for modeling the relativistic diffusion of the quarks.

2.3.1 Random Walk

Consider a one-dimensional random walk with spatial step size l and time step size τ . Let p be the probability to diffuse to the right. ($1 - p$ is then the probability to diffuse to the left.) Then the probability to be at position x at time $t + \tau$ is given by:

$$P_{t+\tau}(x) = pP_t(x - l) + (1 - p)P_t(x + l) \quad (2.29)$$

$$\Rightarrow P_{t+\tau}(x) - P_t(x) = pP_t(x - l) + (1 - p)P_t(x + l) - P_t(x) \quad (2.30)$$

Assuming isotropy, we have $p = 0.5$:

$$P_{t+\tau}(x) - P_t(x) = \frac{1}{2}(P_t(x - l) + P_t(x + l) - 2P_t(x)) \quad (2.31)$$

Those differences can be rewritten as derivatives

$$\tau \partial_t P = \frac{1}{2} l^2 \partial_x^2 P, \quad (2.32)$$

or

$$\partial_t P = D \partial_x^2 P \quad \text{where} \quad D := \frac{l^2}{2\tau} = \frac{1}{2} v l, \quad v := \frac{l}{\tau}. \quad (2.33)$$

D is called *diffusion constant*. This connects the discrete random walk to the continuous diffusion equation.

Let \mathbf{x}_0 denote the initial 4-position of the random walk. Solving the classical diffusion equation for $P(\mathbf{x}|\mathbf{x}_0) = \delta(\mathbf{x} - \mathbf{x}_0)$ gives rise to the *Wiener propagator*

$$P(\mathbf{x}|\mathbf{x}_0) = \frac{1}{\sqrt{4\pi D(t-t_0)}} \exp\left(-\frac{(\vec{x} - \vec{x}_0)^2}{4D(t-t_0)}\right) \quad \text{for } t > t_0. \quad (2.34)$$

In one dimension $P(t, x|t_0, x_0)dx$ gives the probability that a particle that was at position x_0 at time t_0 can be found in the element $[x, dx]$ at time $t > t_0$. Equation 2.34 shows that this probability is never zero, even for $|\vec{x} - \vec{x}_0| > c(t - t_0)$. Thus this propagator violates causality. The following two subsections discuss possible solutions to this problem.

Note that the integral of the propagator over x is independent of time. If we interpret P as a particle density instead of a probability, then this integral describes the net number of particles.

2.3.2 Causal Diffusion Equation

One possible way to make the diffusion equation causal is to introduce a relaxation time t_r .

Assume the *phase space distribution* $f(\mathbf{x}, \mathbf{p})$ cools towards an equilibrium f_e :

$$d_t f = \partial_t f + \mathbf{v} \nabla f = -\frac{f - f_e}{t_r} \quad (2.35)$$

When considering small t_r and oscillating perturbations of f with small wave numbers, this implies the following generalization of Fick's law²:

$$t_r \partial_t \mathbf{j} + \mathbf{j} = -D \nabla n , \quad (2.36)$$

where n is the particle density. Combining this with the continuity equation,

$$\partial_t n + \nabla j = 0 , \quad (2.37)$$

gives the *causal diffusion* equation:

$$t_r \partial_t^2 n + \partial_t n = D \nabla^2 n \quad (2.38)$$

Information propagates at the speed $v = \sqrt{D/t_r}$. For $t_r = 0$ we get the ordinary diffusion equation. This equation is however not causal, because information travels at infinite speed.

There are some shortcomings when applying this approach to relativistic diffusion: The equation exhibits singular (i.e. δ -peaked) diffusion fronts moving with speed v . For a massive particle this implies that a small fraction of the particle carries a large amount of the kinetic energy (much larger than mc^2), which is unlikely to occur in nature. See Dunkel, Talkner, and Hänggi [25] for reference.

2.3.3 Modeling Relativistic Diffusion

2.3.3.1 Derivation of a Relativistic Propagator

The classical diffusion propagator (2.34) violates causality and is not Lorentz-invariant. Dunkel, Talkner, and Hänggi [25] propose a relativistic generalization. A short reproduction of their approach is given here:

² This is sometimes called Maxwell-Cattaneo relation or telegraph equation.

First, consider the classical case. The *action per mass* of a particle traveling from 4-position \mathbf{x}_0 to \mathbf{x} is given by

$$a(\mathbf{x}, \mathbf{x}_0) = \frac{1}{2} \int_{t_0}^t \vec{v}(t')^2 dt , \quad (2.39)$$

where the velocity \vec{v} is approximately constant between the scatterings during diffusion. This becomes minimal if there are no collisions and the velocity is constant $\forall t' \in [t_0, t]$:

$$\vec{v} = \frac{\vec{x} - \vec{x}_0}{t - t_0} \Rightarrow a_-(\mathbf{x}, \mathbf{x}_0) = \frac{1}{2} \frac{(\vec{x} - \vec{x}_0)^2}{t - t_0} . \quad (2.40)$$

In the non-relativistic case the velocity is unbound, so the maximal action a_+ will be infinity. This lets us rewrite the propagator (2.34) as an integral over all possible actions:

$$a(\mathbf{x}, \mathbf{x}_0) \sim \int_{a_-(\mathbf{x}, \mathbf{x}_0)}^{a_+(\mathbf{x}, \mathbf{x}_0)} \exp\left(\frac{a}{2D}\right) da \quad (2.41)$$

Generalizing (2.39), we get the relativistic action

$$a(\mathbf{x}, \mathbf{x}_0) = - \int_{t_0}^t \sqrt{1 - \vec{v}(t')^2} dt' , \quad (2.42)$$

yielding new maximal and minimal a_{\pm} in analogy to before:

$$a_-(\mathbf{x}, \mathbf{x}_0) = -\sqrt{(t - t_0)^2 - (\vec{x} - \vec{x}_0)^2} = -|\mathbf{x} - \mathbf{x}_0| , \quad (2.43)$$

$$a_+(\mathbf{x}, \mathbf{x}_0) = 0 . \quad (2.44)$$

Plugging this into (2.41) gives a relativistic, manifestly Lorentz-invariant generalization of the Wiener propagator:

$$P(\mathbf{x}|\mathbf{x}_0) \sim \begin{cases} \exp\left(\frac{|\mathbf{x} - \mathbf{x}_0|}{2D}\right) - 1 & \text{for } (\vec{x} - \vec{x}_0)^2 \leq (t - t_0)^2 \\ 0 & \text{otherwise} \end{cases} \quad (2.45)$$

The normalization is time-dependent, see [25] for details.

2.3.3.2 Comparison of Propagators

Figure 2.1a compares the different propagators. It is visible that for large times the difference between the relativistic and the non-relativistic variant are small. For smaller diffusion speeds, the difference becomes even smaller (see Figure 2.1b).

The discrete binomial propagator of a random walk agrees very roughly with the propagators. A random walk does not violate causality, because it can respect the finite diffusion speed by choosing only step sizes in space (Δx) and time (Δt) such that $\frac{\Delta x}{\Delta t} \leq 1$.

2.3.3.3 Random Walk vs. Propagator

In Figure 2.2 the two models (relativistic and non-relativistic propagator) are compared with the histogram of a random walk. It can be seen that the models and the simulation roughly agree, especially for a large amount of steps.

This justifies using the random walk to model relativistic diffusion.

2.4 Generating Hadrons

When a diffused quark hits the freezeout surface, hadronization takes place. In this section the production rate of such hadrons is derived, which will be used to generate the hadrons in a Monte Carlo simulation. We know for each hadron from which quark pair it originated, and thus with which other hadrons it is correlated. This enables us to calculate the corresponding balance function.

2.4.1 Hadron Production Rate

In order to calculate the number of hadrons ΔN_α emitted due to a quark diffusing through the freezeout surface, we need to consider the statistical thermal equilibrium first:

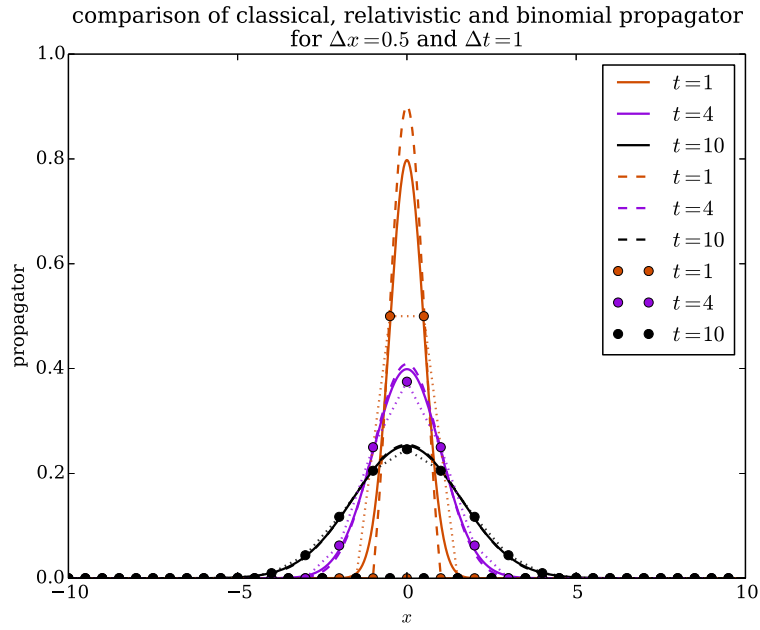
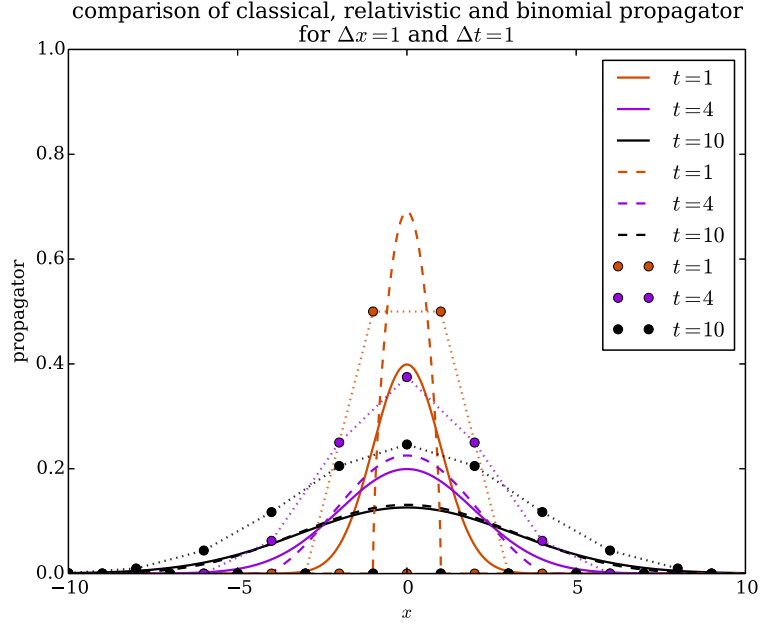
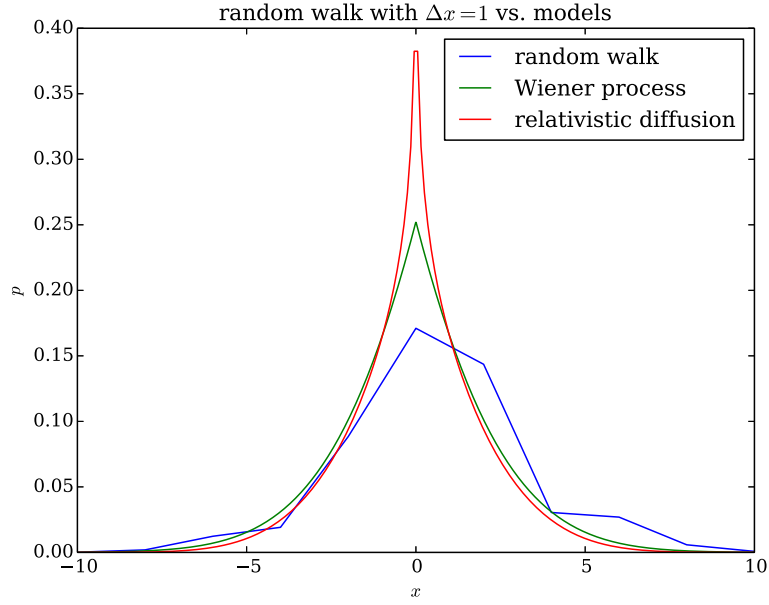
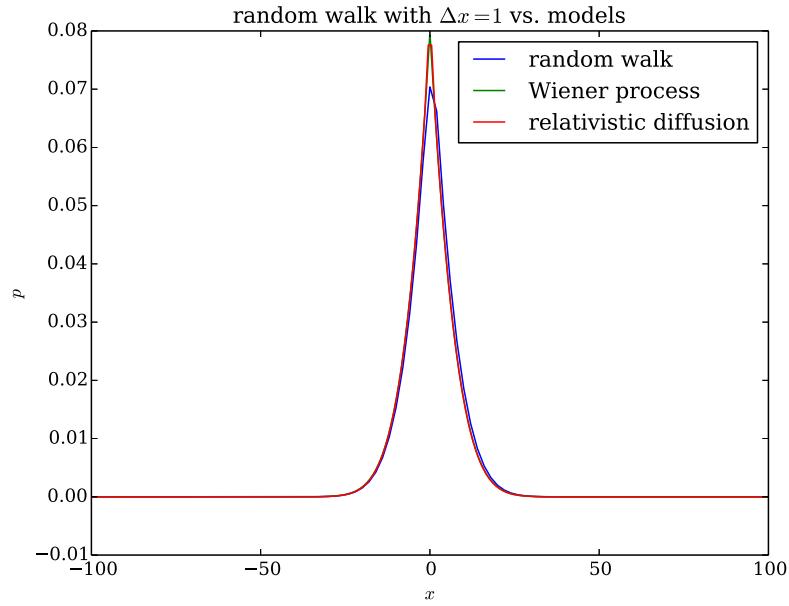


Figure 2.1 Plot of the diffusion propagators as functions of position x and time t for different space and time step sizes Δx and Δt . The continuous lines show the classical Wiener propagator, the dashed lines the generalized relativistic one. The dots show the corresponding binomial probabilities to diffuse from position 0 to x given a random walk. To guide the eye, the dots are connected by dotted lines. Note that the dots have to be compared to the area under the corresponding segment of the continuous propagators. As expected, for smaller Δx the propagators are narrower. Also, the difference between the relativistic and the non-relativistic propagator becomes smaller with decreasing Δx . This is to be anticipated, because the diffusion speed $\Delta x / \Delta t = 0.5$ is smaller than before ($\Delta x / \Delta t = 1$).



(a) 10 random steps.



(b) 100 random steps.

Figure 2.2 Plot of probability p to end up at position x after a one-dimensional random walk. The blue line is a histogram for x after the specified amount of steps. The green line is the classical propagator integrated in time, the red line the relativistic one integrated in time. While the relativistic propagator is narrower and actually vanishes at the maximal possible x , the results are very similar. For a high amount of random steps, the random walk histogram is very close to the propagators.

Thermal equilibrium can be formulated as a constrained entropy maximization. Mathematically this requires *Lagrange multipliers*. For probabilities f_i the Gibbs entropy is given by $\sum_i f_i \log f_i$, which has to be maximized while conserving the following quantities:

1. total probability $\sum_i f_i$,
2. average energy ϵ and
3. charge flux through the freezeout surface

with corresponding Lagrange multipliers α, β, γ .

$$\max_{f_i} - \sum_i \left(f_i \log f_i + \alpha f_i + \beta f_i \epsilon_i + \gamma q \frac{f_i}{\epsilon_i} \mathbf{p}_i \cdot \mathbf{\Omega} \right) \quad (2.46)$$

$$\Rightarrow 0 = - \sum_i \left(\log f_i + 1 + \alpha + \beta \epsilon_i + \gamma q \frac{\mathbf{p}_i \cdot \mathbf{\Omega}}{\epsilon_i} \right) \quad (2.47)$$

$$\Leftrightarrow \prod_i f_i = \exp \left(-1 - \alpha - \beta \sum_i \epsilon_i - \gamma q \sum_i \frac{\mathbf{p}_i \cdot \mathbf{\Omega}}{\epsilon_i} \right) \quad (2.48)$$

(Note that $\mathbf{p} \cdot \mathbf{\Omega} = E_p \Omega_0 - \vec{p} \vec{\Omega}$.)

This means that the requirement of the conservation of charge flux through the hypersurface introduces a factor of $\exp(\gamma q \mathbf{p} \cdot \mathbf{\Omega} / E_p)$. We need to consider different quark species a , so the γ term should depend on a .

Consequently we get the change in the number of hadron species α in terms of the a -quark charge $q_{\alpha,a}$ of the hadron and the Lagrange multiplier γ :

$$d(\Delta N_\alpha) = dN_\alpha \left(\exp \left(\sum_a \gamma_a \frac{\mathbf{p} \cdot \mathbf{\Omega}}{E_p} q_{\alpha,a} \right) - 1 \right) \quad (2.49)$$

$$\approx dN_\alpha \sum_a \gamma_a \frac{\mathbf{p} \cdot \mathbf{\Omega}}{E_p} q_{\alpha,a} \quad (2.50)$$

(If we consider $\mathbf{p} \cdot \mathbf{\Omega}/E_p = 1$ in the exponential correction, then we obtain N_α instead of ξ_α . The multiplier γ_a is then usually defined terms of the change in chemical potential $\Delta\mu_a$ and temperature T :

$$\gamma_a \Big|_{\mathbf{p} \cdot \mathbf{\Omega}/E_p=1} = \frac{\Delta\mu_a}{T} \quad (2.51)$$

This yields

$$d(\Delta N_\alpha) \approx dN_\alpha \sum_a \frac{\Delta\mu_a q_{\alpha,a}}{T} \quad (2.52)$$

instead.)

In our case, dN_α can be calculated using the momentum distribution f_α and the Cooper-Frye formula [23]:

$$dN_\alpha = \frac{1}{(2\pi)^3} \frac{d^3p}{E_p} \mathbf{p} \cdot \mathbf{\Omega} f_\alpha(\mathbf{p}) \quad \text{where} \quad \mathbf{p} = (E_p, \vec{p}) \quad (2.53)$$

Substituting this gives:

$$\xi_\alpha := \frac{1}{(2\pi)^3} \int d^3p f_\alpha(\vec{p}) \left(\frac{\mathbf{p} \cdot \mathbf{\Omega}}{E_p} \right)^2 \quad \text{where} \quad f_\alpha(\vec{p}) := g e^{-\frac{\mathbf{u} \cdot \mathbf{p}}{T}} = g e^{-\frac{E_p}{T}} \quad (2.54)$$

$$\hat{\chi}_{ab} := \sum_\alpha \xi_\alpha q_{\alpha,a} q_{\alpha,b} = \hat{\chi}_{ba} \quad (2.55)$$

$$\Delta N_\alpha = \xi_\alpha q_{\alpha,a} \gamma_a \quad (2.56)$$

Note that the normal phase space density contributes one factor of $\mathbf{p} \cdot \mathbf{\Omega}/E_p$, the additional Lagrange multiplier γ (corresponding to the conservation of charge through the freezeout surface) contributes another one. This additional factor is the difference in the definition of χ_{ab} compared to subsection 2.2.1, where $\langle N_\alpha \rangle$ as used instead of ξ_α . The moment distribution f_α chosen here is proportional to the degeneracy g and will be discussed in the next section.

Conservation of b -quark charge q_b demands that

$$\Delta Q_b = \sum_{\alpha} q_{\alpha,b} \Delta N_{\alpha} \quad (2.57)$$

$$\approx \sum_{\alpha,a} \xi_{\alpha} \gamma_a q_{\alpha,b} q_{\alpha,a} \quad (2.58)$$

$$= \sum_a \hat{\chi}_{ba} \gamma_a . \quad (2.59)$$

Inverting the matrix product yields the Lagrange multiplier

$$\gamma_a = \sum_b \hat{\chi}_{ab}^{-1} \Delta Q_b , \quad (2.60)$$

which can be substituted into the initial expression:

$$\Delta N_{\alpha} = \xi_{\alpha} \sum_{ab} \hat{\chi}_{ab}^{-1} q_{\alpha,a} \Delta Q_b \quad (2.61)$$

Here ΔN_{α} is the additional number of α hadrons due to an extra charge ΔQ_b flowing through the hypersurface. Note that for antiparticles $\bar{\alpha}$ we have $\Delta N_{\bar{\alpha}} = -\Delta N_{\alpha}$, and that ΔN is independent of the magnitude of the hypersurface element, because $\xi \sim |\Omega|$ and $|\chi^{-1}| \sim \xi^{-1} \sim |\Omega|^{-1}$.

2.4.2 Maxwell-Jüttner Distribution

In the previous subsection an expression for the hadron production rate at the freezeout surface was derived. To be able to calculate it, we need to choose an appropriate momentum distribution f_{α} .

After the freezeout the densities should be low enough that we can assume the hadrons are non-interacting particles in thermal equilibrium. In this case, the momentum follows the *Maxwell-Jüttner distribution* [26], a relativistic generalization of the Maxwell-Boltzmann

distribution:

$$f(\mathbf{p}) = \frac{g}{e^{(\mathbf{u} \cdot \mathbf{p} - \mu)/T} + \lambda} \quad (2.62)$$

where g is the *degeneracy*, μ the *chemical potential* in equilibrium and

$$\lambda = \begin{cases} 1 & \text{for Fermi-Dirac} \\ -1 & \text{for Bose-Einstein} \\ 0 & \text{for Maxwell-Boltzmann} \end{cases} \quad (2.63)$$

statistics. Note that the degeneracy for a spin s particle is given by the number of possible spin states:

$$g = 2s + 1 \quad (2.64)$$

Assuming the ultrarelativistic case $e^{\mathbf{u} \cdot \mathbf{p}/T} \gg 1$ and $\mathbf{u} \cdot \mathbf{p} \gg \mu$, Equation 2.62 simplifies to the Maxwell-Boltzmann distribution:

$$f(\mathbf{p}) = g e^{-\mathbf{u} \cdot \mathbf{p}/T} \quad (2.65)$$

For pions, the Bose-Einstein distribution would differ at the 5% level. Integrating gives the average particle number:

$$n = \int f(\mathbf{p}) \frac{d^3 p}{(2\pi)^3} = \frac{gd}{(2\pi)^3} \quad \text{where} \quad d := 4\pi T m^2 K_2\left(\frac{m}{T}\right) \quad (2.66)$$

where K_2 a modified Bessel function of the second kind, defined more generally [27, 28] by the integral

$$\forall a > -\frac{1}{2}: \quad K_a(\zeta) := \left(\frac{\zeta}{2}\right)^a \frac{\Gamma(\frac{1}{2})}{\Gamma(a + \frac{1}{2})} \int_1^\infty e^{-\zeta y} (y^2 - 1)^{a - \frac{1}{2}} dy. \quad (2.67)$$

(Note that $\Gamma(\frac{1}{2}) = \sqrt{\pi}$.) See section 4.2 for the derivation of the normalization d .

2.4.3 Hadron Production Rate – Continued

Now that we have picked a momentum distribution f_α , we can calculate the integral from subsection 2.4.1:

$$\zeta_\alpha := \frac{g}{(2\pi)^3} \int d^3p \left(\frac{\mathbf{p} \cdot \boldsymbol{\Omega}}{E_p} \right)^2 \exp \left(-\frac{\mathbf{u} \cdot \mathbf{p}}{T} \right) \quad (2.68)$$

$$= \frac{\Omega_0^2 g d}{(2\pi)^3} + \frac{g}{(2\pi)^3} \int d^3p \left(\frac{p_z \Omega_z}{E_p} \right)^2 e^{-\frac{E_p}{T}} \quad (2.69)$$

Without loss of generality, we chose coordinates where

$$\mathbf{u} = (1, 0, 0, 0) \quad \text{and} \quad \boldsymbol{\Omega} = (\Omega_0, 0, 0, \Omega_z) . \quad (2.70)$$

See Equation 2.66 for the definition of d . Since the integral is symmetric to the choice of z , we can replace p_z with p :

$$\zeta_\alpha = \frac{\Omega_0^2 g d}{(2\pi)^3} + \frac{\Omega_z^2 g}{3(2\pi)^3} \int d^3p \frac{p^2}{E_p^2} e^{-\frac{E_p}{T}} \quad (2.71)$$

This integral is similar to the normalization of the Jüttner distribution. The same coordinate transformation can be used here:

$$\int d^3p \frac{p^2}{E_p^2} e^{-\frac{E_p}{T}} = 4\pi \int_0^\infty \frac{p^4}{E_p^2} e^{-\frac{E_p}{T}} dp = 4\pi m^3 \int_1^\infty \frac{(\gamma^2 - 1)^{3/2}}{\gamma} e^{-\frac{m}{T}\gamma} d\gamma \quad (2.72)$$

If it weren't for the factor $1/\gamma$, this could be expressed as a modified Bessel function using (2.67).

Mathematica [29] could not compute this integral. SymPy [30] returns a result in terms of Meijer G-functions [31]:

$$\int_1^\infty \frac{(\gamma^2 - 1)^{3/2}}{\gamma} e^{-\frac{m}{T}\gamma} d\gamma = \frac{3}{8} G_{1,3}^{3,0} \left(\begin{matrix} 1 \\ -\frac{3}{2}, 0, \frac{1}{2} \end{matrix} \middle| \frac{m^2}{4T^2} \right) \quad (2.73)$$

where

$$G_{p,q}^{m,n} \left(\begin{matrix} a_1, \dots, a_p \\ b_1, \dots, b_q \end{matrix} \middle| z \right) := \frac{1}{2\pi i} \int_L \frac{\prod_{j=1}^m \Gamma(b_j - s) \prod_{j=1}^n \Gamma(1 - a_j + s)}{\prod_{j=m+1}^q \Gamma(1 - b_j + s) \prod_{j=n+1}^p \Gamma(a_j - s)} z^s ds \quad (2.74)$$

for

- $m, n, p, q \in \mathbb{Z} : \quad m \in [0, q], n \in [0, p]$
- $a_k - b_j \notin \mathbb{N} \quad \forall k \in \{1, \dots, n\}, j \in \{1, \dots, m\}$
- $z \neq 0$.

L represents the line in the complex plane along which the integration is performed. There are three different options, see [31] for more details.

In practice it is difficult to find implementations that numerically calculate the Meijer G-function. Since implementing them is non-trivial, the easiest approach to evaluate ξ_α is numerical integration. We are only interested in ξ_α at the freezeout surface, so we can get away with calculating the integral only once for every hadron species.

2.4.3.1 Non-Relativistic Limit

In the non-relativistic limit the temperature is much smaller than the mass of the hadron:

$$T \ll m \quad \Rightarrow \quad \frac{p}{E_p} \approx v \quad (2.75)$$

We can also assume the hadrons behave like an ideal gas. The *equipartition theorem* then gives

$$\frac{1}{2} m \langle v^2 \rangle = \frac{3}{2} T \quad \Leftrightarrow \quad \langle v^2 \rangle = \frac{3T}{m} \quad (2.76)$$

Applying those results to (2.69):

$$\frac{\xi_\alpha}{g} = \frac{\Omega_0^2 d}{(2\pi)^3} + \frac{\Omega_z^2}{3(2\pi)^3} \int d^3 p \frac{p^2}{E_p^2} f_\alpha(p) \quad (2.77)$$

$$\approx \frac{\Omega_0^2 d}{(2\pi)^3} + \frac{\Omega_z^2 d}{3(2\pi)^3} \langle v^2 \rangle \quad (2.78)$$

$$= \frac{\Omega_0^2 d}{(2\pi)^3} + \frac{\Omega_z^2 d}{(2\pi)^3} \frac{T}{m} \quad (2.79)$$

2.4.3.2 Ultra-Relativistic Limit

In the ultra-relativistic limit the temperatures is much higher than the hadron mass:

$$T \gg m \quad \Rightarrow \quad \frac{p}{E_p} \approx 1 \quad (2.80)$$

This makes the integral very simple:

$$\xi_\alpha = \frac{\Omega_0^2 g d}{(2\pi)^3} + \frac{\Omega_z^2}{3(2\pi)^3} \int d^3 p \frac{p^2}{E_p^2} f_\alpha(p) \quad (2.81)$$

$$\approx \frac{\Omega_0^2 g d}{(2\pi)^3} + \frac{\Omega_z^2 g d}{3(2\pi)^3} \quad (2.82)$$

Now we know how to calculate ξ_α and thus ΔN_α from the diffused thermal quarks. This concludes the theoretical chapter. In the next chapter we will apply these results to implement a Monte Carlo simulation that outputs the generated hadrons, which can be used to calculate balance functions.

Chapter 3

Implementation

This chapter discusses the implementation of the microscopic model derived in the previous chapter. Section 3.1 shows how the lattice quantum chromodynamics data can be combined with the hydrodynamics data to calculate the quark pair source function and how quarks are generated from this result. In section 3.2, technical implementation details of the random walk algorithm and the freezeout detection are discussed. Section 3.3 describes how the quark freezeout events can be translated into hadrons. Section 3.4 gives a brief description how the hadron cascade was implemented, and finally section 3.5 explains how the balance functions can be calculated.

3.1 Generation of Quark Pairs

To calculate the number of generated quark pairs (2.26), we need to know the charge fluctuations χ_{ab} . Quantum chromodynamics simulations using lattice gauge theory give the charge fluctuation over entropy χ/s as a function of temperature T (see Figure 3.1 and [32]). The limits are what we would expect from subsection 2.2.1: For high temperatures we expect a parton gas (2.14); χ should be diagonal and constant in temperature. Similarly for low temperatures there should be a hadron gas (2.13) dominated by mesons, because they are lighter than baryons. This explains the negative off-diagonal term. Pions

are lighter and thus more common than kaons, explaining that χ_{uu} is higher χ_{ss} .

Unfortunately the lattice QCD data is not available for all the off-diagonal elements of χ . For low temperatures the densities are very low, so it makes sense to assume a hadron gas that follows the thermal distribution discussed in subsection 2.4.2. The particle density is then given by the Jüttner distribution (2.66). χ is then given by Equation 2.13. For high temperatures we can assume a parton gas and the off-diagonal terms should vanish as discussed above. Similarly the entropy can be calculated.

Those observations lead to the following approach to approximate χ :

- For diagonal terms, use the lattice data for temperatures above 200 MeV. Linearly interpolate χ/s as given by the hadron gas at 165 MeV and the lattice data at 200 MeV otherwise.
- For off-diagonal terms, set χ to zero above 200 MeV. Linearly interpolate χ/s as given by the hadron gas at 165 MeV and 0 at 200 MeV otherwise.

The lattice data is only available for a finite sample of temperatures (that is, every 5 MeV between 130 and 400 MeV). Values for temperatures in between those samples can be interpolated using cubic splines.

An Israel-Stewart hydrodynamics code [33] gives the temperature, the entropy and the velocity as a function of space and time (see Figure 3.2 for an example). The initial conditions chosen when running the code represent the parameters of the collision (centrality, collision energy, etc.). While the code is capable of running in three dimensions, for our case we are interested in the relativistic limit, where the hydrodynamics is approximately two-dimensional due to boost invariance. This means that we only need to consider the hydrodynamic data in the transverse plane. Furthermore, the code can exploit elliptical symmetry by only considering one octant of the coordinate system.

Given the temperature, we can now calculate χ using the approach described above. Plugging this in, the fluid velocity and the entropy into Equation 2.26 gives the source

function for thermal pairs of a quark and an anti-quark.¹ Assuming a Poisson distribution, this serves as the number of particles that need to be generated.

A generated quark provides an additional charge to the net neutral quark gluon plasma. The source function can be negative, in which cases negative weight particles can be generated, corresponding to quark holes in the plasma. The partner quarks are generated at the same point in spacetime and will be diffused apart as described in the next section.

For each timestep, each hydro cell and each quark species pair, we are given a positive real number N representing the number of particles to generate (the source function). The following algorithm² is an efficient way to decide how many particles to generate:

1. Set $\zeta := 0$.
2. Uniformly draw a random number $r \in [0, 1]$. Increase ζ by $-\log r$.
3. If $N > \zeta$, then create a quark pair and go to 2. Otherwise halt.

This way the quarks are generated according to a poissonian distribution. Their exact position can be randomly picked from the corresponding hydro cell (using a uniform distribution). Now that we have generated the quarks, we can go on to the next step and diffuse them apart.

3.2 Diffusion of Quarks

As motivated in section 2.3, the thermal quarks are then diffused by performing a random walk in three dimensions. (Because our hydrodynamics data is two-dimensional, we need to project to the transverse plane if we need hydrodynamic quantities.) Relativity is respected by making sure that none of the steps are faster than the speed of light. The quarks

¹ It is equivalently possible to generate pairs of quarks or pairs of anti-quarks, the weights would have to be adapted. Consider for instance generating an up and an anti-down quark. Then $\chi_{u\bar{d}}$ will be positive and $g_{\pi^+\pi^+}$ should be as well. So the weight has to be 1. Analogously, when generating an up and a down quark the weight has to be -1.

² See [22] for similar algorithm that scales well for many different species.

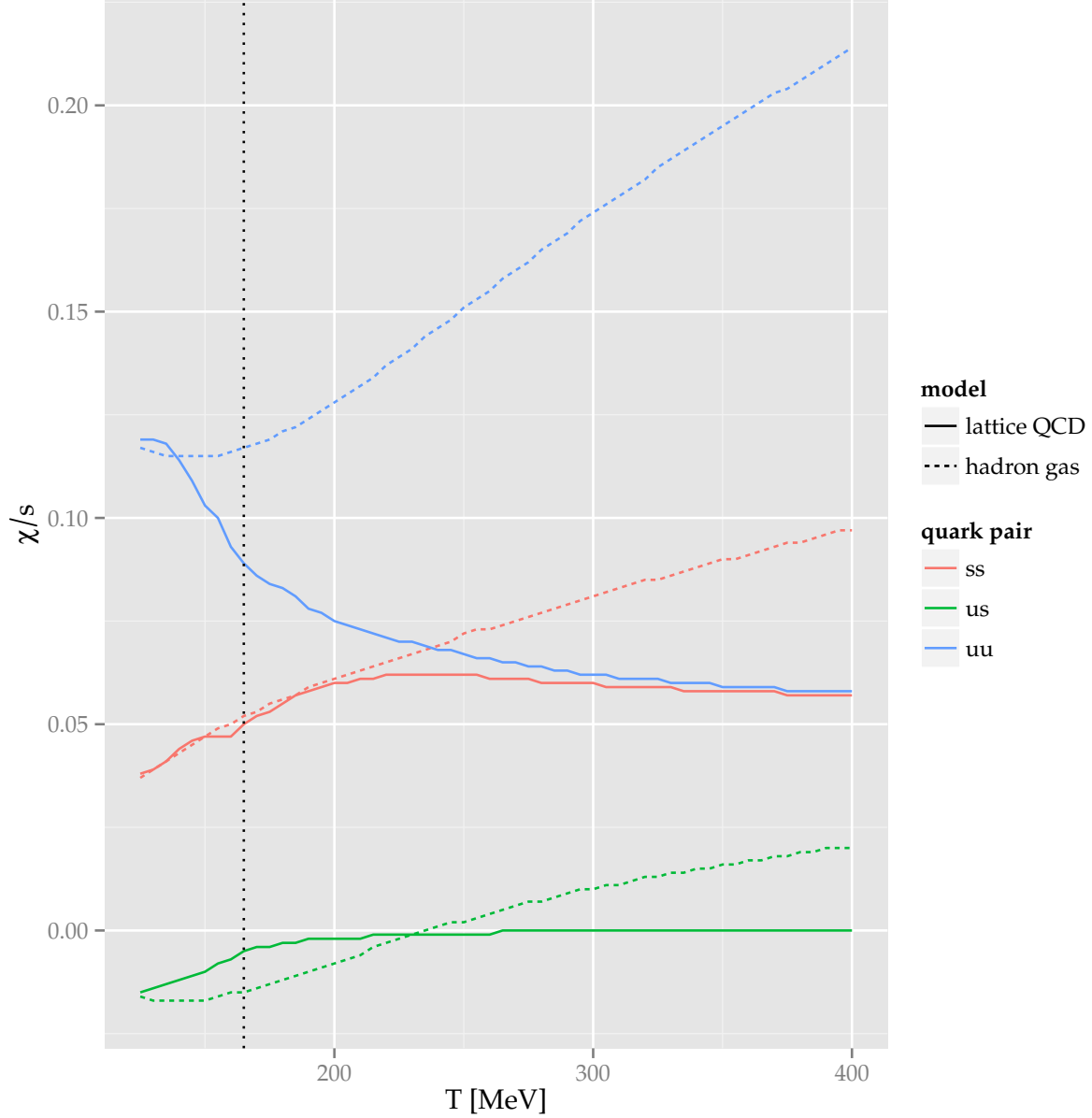


Figure 3.1 Charge fluctuation χ over entropy s as a function of temperature T for various quark pairs. The dotted vertical line represents the freezeout temperature at 165 MeV. The solid lines represent the results of lattice QCD simulations of a quark-gluon plasma [32]. The dashed lines show the results of assuming a hadron gas in thermal equilibrium (2.13). Note that for high temperatures χ/s is roughly constant according to lattice QCD, and the offdiagonal element (χ_{us}) vanishes as expected for the parton gas model (2.14). The hadron gas model roughly agrees with the lattice data for small temperatures. For high temperatures it does not, in that limit we expect the plasma to behave like a parton gas where all light species are the same, because their masses are significantly smaller than the temperature ($m_u \approx m_d \ll m_s \approx 100$ MeV). This expectation is confirmed by the lattice data.

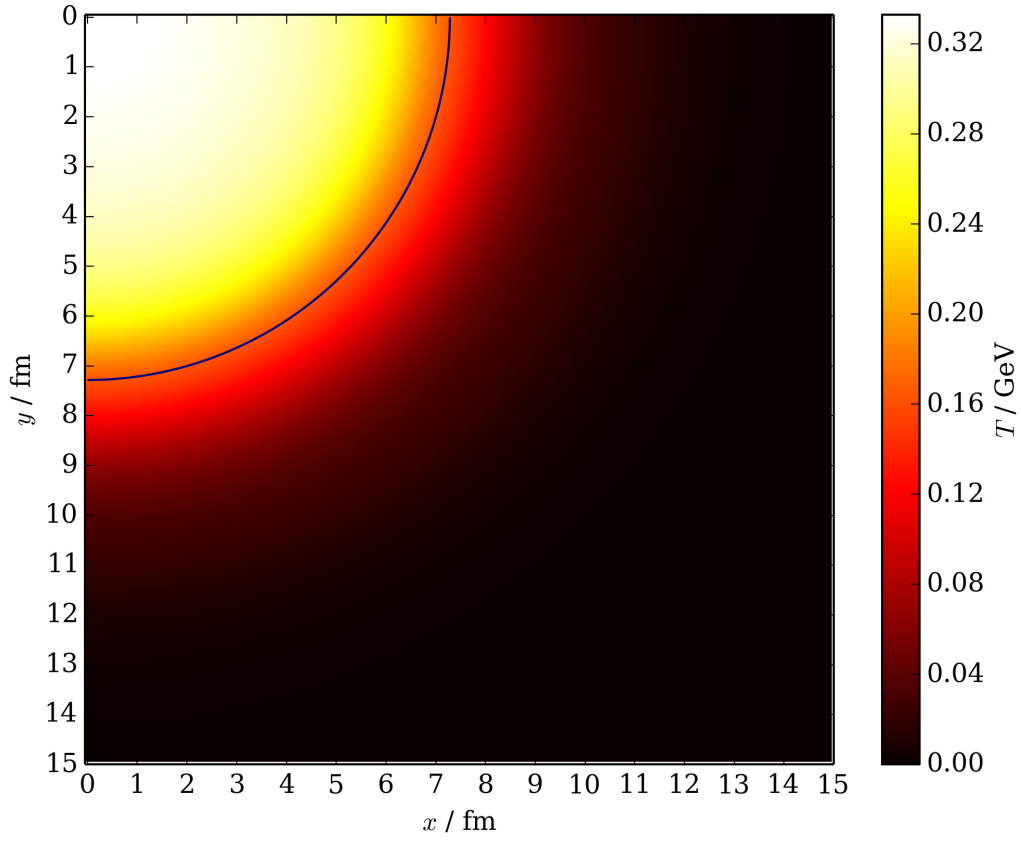


Figure 3.2 Temperature T as a function of space (x, y) in the transverse plane. The solid line represents the freezeout temperature at 165 MeV. This was taken at the beginning of an Israel-Stewart hydrodynamics simulation (see [33] for the implementation).

are boosted into the restframe of the fluid (whose velocity is given by the hydrodynamics data), displaced by a random step in a random direction, and boosted back into the lab frame. See Figure 3.3 for an illustrating plot of such a random walk.

Anytime during this diffusion step, the temperature might fall below freezeout. To detect this, a line is traced between the starting point and the end point of the diffusion. The crossed hydro cells can be efficiently computed using a variant of the Bresenham algorithm [34], which was designed to efficiently render lines on a raster. See Figure 3.4 for an illustration. This yields all the relevant temperatures to consider for freezeout. By interpolating time linearly, we can check the temperature for all fluid elements of the trajectory (within the limited resolution of the hydrodynamics data). In the end, this gives a list of all quark freezeout events.

3.3 Hadronization

Whenever a quark (or quark hole) hits the freezeout surface, we get an additional quark charge (positive or negative). This can be correlated to the generation of a hadron using this equation (see subsection 2.4.1):

$$\Delta N_\alpha = \xi_\alpha q_{\alpha,a} \hat{\chi}_{ab}^{-1} \Delta Q_b \quad (3.1)$$

where

$$\xi_\alpha = \frac{g}{(2\pi)^3} \int d^3p \left(\frac{\mathbf{p} \cdot \mathbf{\Omega}}{E_p} \right)^2 e^{-E_p/T} \quad \text{and} \quad \hat{\chi}_{ab} = \sum_\alpha \xi_\alpha q_{\alpha,a} q_{\alpha,b} . \quad (3.2)$$

α represents the hadron species with all the associated properties (mass, charge, degeneracy). In theory, α can be any known hadrons species. In practice, we are considering 319 different species. While most of those are generated in negligible quantities, they are still considered in the simulation. The change in b -charge ΔQ_b is given by the quark freeze-out event. For a negative weight quark (a quark hole), ΔQ_b has the opposite sign compared

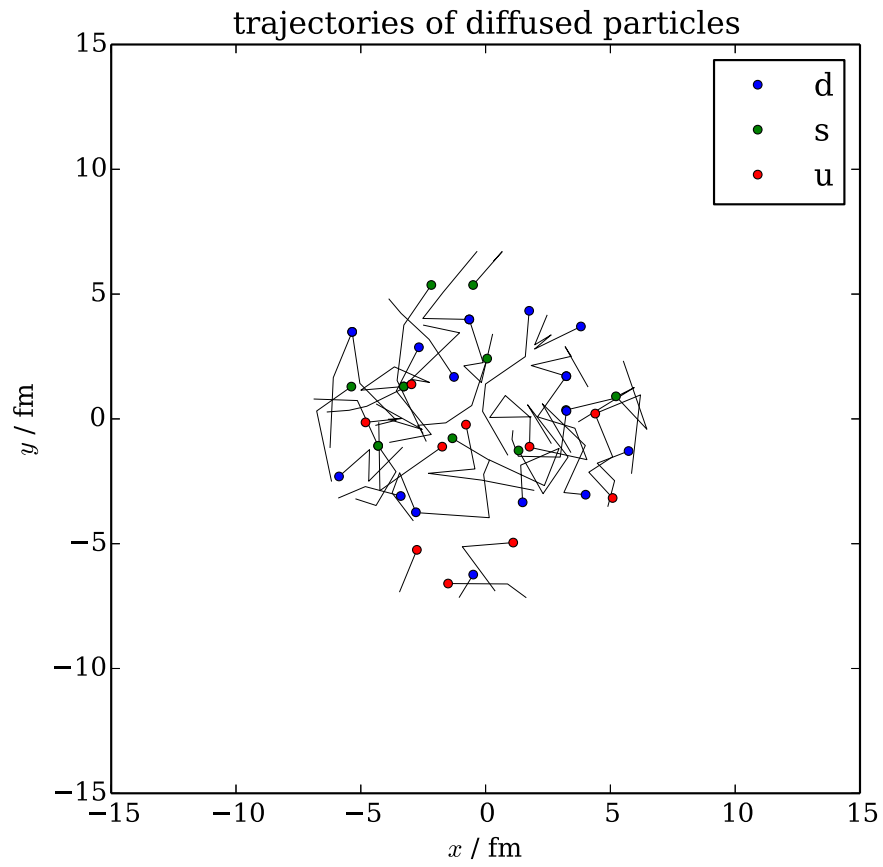


Figure 3.3 Example of a random walk as implemented here. This shows the diffusion trajectories of a random sample of quarks from the first population until they freeze out. The trajectories are projected to the transverse plane.

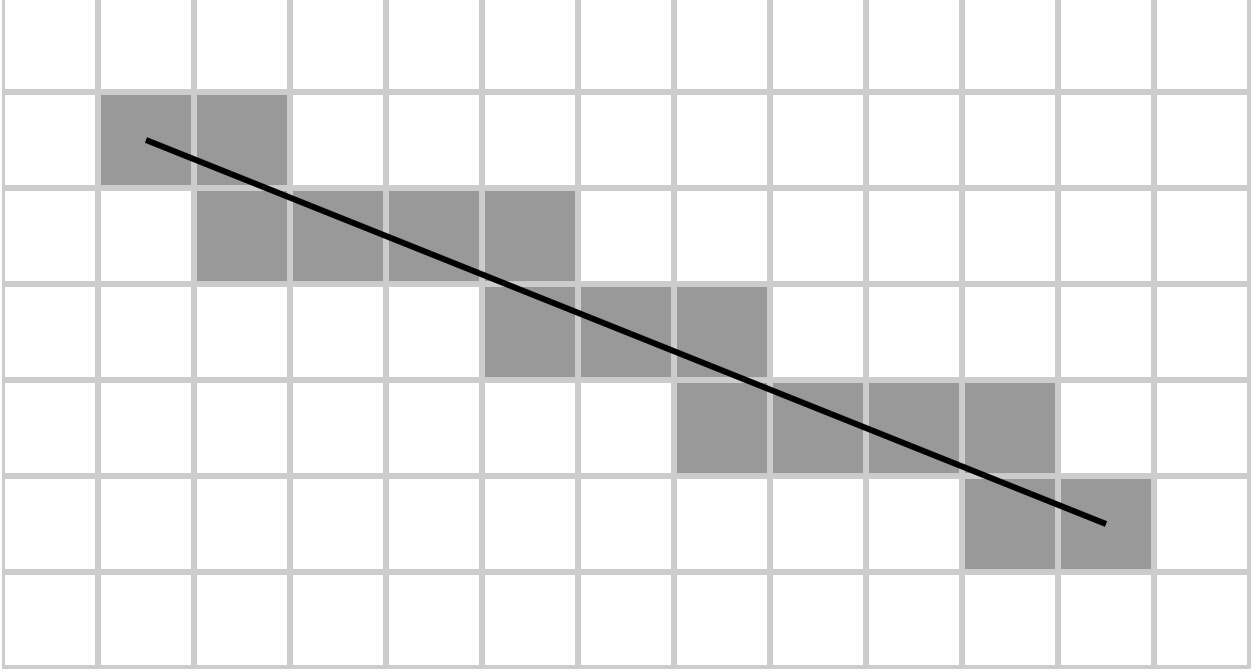


Figure 3.4 An illustration of the modified Bresenham algorithm used. Each square cut by the diffusion trajectory has to be considered, because it is a possibility for a freezeout.

to a positive weight quark. The a -charge $q_{\alpha,a}$ is a property of the hadron species α . The surface element Ω^μ must be proportional to the temperature 4-gradient $\partial^\mu T$. ΔN_α is invariant to the normalization of Ω^μ (see subsection 2.4.1). When assuming thermal equilibrium, f_α is given by the Jüttner distribution (see subsection 2.4.2), which depends on the mass of the species and the (freezeout) temperature.

It is not clear at which temperature the freezeout occurs. Plausible values range from 130 MeV to 175 MeV [35], the exact value is essentially a parameter of the model. For the calculations done here, a freezeout temperature of 165 MeV was chosen. It is worth mentioning that the cascade can compensate for an earlier freezeout.³

Using all this, ξ_α , $\hat{\chi}_{ab}$, and thus ΔN_α can be calculated. Because we can pull the Ω out of the integral and T is constant, the integral in ξ_α needs to be calculated only once for every species α . $\hat{\chi}_{ab}^{-1}$ has to be recalculated for every quark freezeout event, because it depends

³ An example: Choosing a freezeout temperature of 165 MeV yields about as many ρ mesons as protons. Rho mesons are unstable and decay rather quickly when performing the hadron cascade. If we choose a freezeout temperature of 130 MeV instead, then there are only few rho mesons compared to protons after the freezeout.

on the hypersurface element Ω . Since $\hat{\chi}_{ab}$ is only a 3-by-3 matrix, inverting it is not very expensive. The resulting ΔN_α can be used to generate hadrons in the same fashion as the quarks were generated.

Additionally, a momentum from f_α has to be drawn, which can be done using rejection sampling: It is easy to generate a momentum that is exponentially distributed (by taking the log of a uniformly random number). To honor the remaining coefficient in the integral we need to find a weight to do rejection sampling. This can be done by factoring out an arbitrary constant Ω_{max} , such that we obtain the weight

$$w := \left(\frac{\mathbf{p} \cdot \mathbf{\Omega}}{E_p \Omega_{max}} \right)^2. \quad (3.3)$$

To minimize rejection (rejecting often hurts the performance of the program), we should pick an Ω_{max} that maximizes $w \in [0, 1]$. For this we need to find the upper bound of the following expression:

$$\left| \frac{\mathbf{p} \cdot \mathbf{\Omega}}{E_p} \right| = \left| \Omega_0 - \frac{\vec{p}}{E_p} \cdot \vec{\Omega} \right| = \left| \Omega_0 - \frac{|\vec{p}|}{\sqrt{m^2 + \vec{p}^2}} |\vec{\Omega}| \cos \theta \right| \quad (3.4)$$

$$\leq |\Omega_0| + |\vec{\Omega}| =: \Omega_{max} \quad (3.5)$$

$$= |\mathbf{\Omega} \cdot \mathbf{u}| + \sqrt{(\mathbf{\Omega} \cdot \mathbf{u})^2 - \mathbf{\Omega}^2} \quad (3.6)$$

This result can then be used to generate the correct momentum using the following algorithm:

1. Draw momentum from $f(p) \sim \exp(-\frac{Ep}{T})$.
2. Calculate w . Uniformly draw a number $r \in [0, 1]$. If $r > w$, reject the momentum and go back to 1. Keep the momentum otherwise.

Now we have determined all the properties of the hadron we need: The momentum was just calculated, and the position in spacetime is given by the freezeout event. Before

being able to calculate the balance functions that correspond to the experimental measurements, the hadrons need to scatter and decay in the cascade.

Efficient Calculation of ζ and $\hat{\chi}$ This paragraph discusses some technical details that help to avoid calculating ζ and $\hat{\chi}$ more often than necessary. While ζ_α needs to be calculated for every hypersurface element Ω , it can be separated in parts depending only on α and parts depending only on Ω :

$$\zeta_\alpha =: \Omega_0^2 I_{1,\alpha} + \Omega_z^2 I_{2,\alpha} \quad (3.7)$$

Similarly, we can separate $\hat{\chi}$:

$$\hat{\chi}_{ab} = \sum_\alpha \zeta_\alpha q_{\alpha,a} q_{\alpha,b} = \sum_\alpha \left(\Omega_0^2 I_{1,\alpha} + \Omega_z^2 I_{2,\alpha} \right) q_{\alpha,a} q_{\alpha,b} =: \Omega_0^2 A_{1,ab} + \Omega_z^2 A_{2,ab} \quad (3.8)$$

The scalars $I_{i,\alpha}$ and the matrices A_i can be calculated for every species once, as long as the temperature is constant. Since we are only interested in calculating $\hat{\chi}$ at the freezeout surface, this condition is met.

3.4 Hadron Cascade

The hadrons that froze out after the quarks hit the freezeout surface do not yet correspond to what one would observe in experiment. To get rid of unstable hadrons (e.g. rho mesons), it is still necessary to simulate their decays and to scatter them with each other. For this the *b3d* code described in reference [20] has been used. After this, the hadrons have reached their final state and the balance functions can be calculated.

3.5 Calculating Balance Functions

As mentioned in the beginning of chapter 2, there are two contributions to be considered in order to calculate the balance functions: The contribution due to the generated quark

pairs above the freezeout temperature (which has been discussed in this thesis), and the contribution due to uncorrelated hadrons in the cascade that annihilate each other (which has been implemented in the *b3d* code).

For comparison with experimental data, it is important to consider the selectivity and efficiency of the corresponding detector. Because the model yields individual hadrons, it is straightforward to apply these constraints and include the efficiencies in the calculation.

3.5.1 Contribution above Freezeout Temperature

We are mainly interested in the fate of the quark pair: how it separated and hadronized and how the resulting hadrons were propagated through the cascade. This gives us the hadronic balance functions, because we know which hadrons are correlated and how far they separated by tracing them back to their quark origin.

For each quark a number of hadrons from 0 to ∞ can be generated. Since we expect ΔN_α to be small, this means that we are likely to get a lot of hadrons without a partner, reducing the amount of useful data. In practice this means that about 80% of the generated hadrons don't have a partner.

The propagation of the correlated hadrons through the cascade and the calculation of the resulting balance function contribution was handled by collaborators.

3.5.2 Contribution below Freezeout Temperature

It is possible to generate uncorrelated hadrons using the momentum distribution of a relativistic gas (similar to what has been discussed in subsection 2.4.2). These hadrons can be decayed and scattered as for the hadrons originating in the generated quark pairs from the previous contribution. Annihilations need to be included, because they contribute to the charge balance function. Again, the *b3d* code is used.

After that, the balance functions can be calculated by iterating over all possible hadron

pairs, calculating their separation in rapidity and filling histograms corresponding to the pairs. If a negative weight particle is encountered, the count in the corresponding bin has to be decreased instead of increased. Recalling the definition of the balance function allows us to calculate the numerator directly from these histograms:

$$B_{\alpha\beta}(\Delta y) \sim \langle (N_\alpha - N_{\bar{\alpha}})(N_\beta - N_{\bar{\beta}}) \rangle(\Delta y) \quad (3.9)$$

$$= \langle N_\alpha N_\beta \rangle(\Delta y) - \langle N_\alpha N_{\bar{\beta}} \rangle(\Delta y) - \langle N_{\bar{\alpha}} N_\beta \rangle(\Delta y) + \langle N_{\bar{\alpha}} N_{\bar{\beta}} \rangle(\Delta y) \quad (3.10)$$

Dividing this by the total number of β and $\bar{\beta}$ hadrons then yields the the balance function.

Chapter 4

Conclusion

4.1 Summary

We have developed a model that will provide quantitative predictions of the number of quark-antiquark pairs generated during the evolution of a relativistic heavy ion collision. The production rate depends on results of lattice gauge theory for charge susceptibilities and on the hydrodynamic evolution which provides the entropy density and temperature profiles. The separation of the correlated quarks was modeled using a diffusive process by employing a random walk for each individual quark. Care was taken to ensure that causality was not violated in the description. These correlations were propagated through a hadronization formula across an interface between the hydrodynamic description and a hadronic cascade modeling the breakup and dissolution of the fireball. The correlations from the initial charge conservation were tracked through the cascade and summed alongside correlations from decays and annihilations during the cascade. The final-state correlations were quantified in the form of charge balance functions, which can be compared to experiment.

Once the approach is better tested and the responses of the experimental detectors are accurately incorporated, the results from this approach should give profound insight into

the chemical evolution of the quark-gluon plasma. Charge balance functions have been shown to be sensitive to both the chemical make-up of the quark-gluon plasma and the diffusion. We hope that this approach will provide quantitative answers to the question of whether the matter formed in relativistic heavy ion collisions had the same numbers of up, down and strange quarks as the equilibrated matter studied in lattice gauge theory. Further, one may even be able to extract the diffusion constant of the quark-gluon plasma, a fundamental transport coefficient that has thus far not been addressable either through experiment or by lattice calculations.

4.2 Future Work

The model shown here represents the field's first attempt to microscopically model the evolution of charge correlations. Most of the pieces of the approach are now in place, but significant work is required to complete the model and to validate that it indeed faithfully represents the equations described here. Once finished, the model will address a variety of measurements in a way that provides insights into the chemical evolution of a heavy-ion collision. A list of short-term goals is presented here:

Testing the Model The model has not yet been extensively tested for self-consistency. For instance, it should be ensured that the balance functions for electric charge and baryon number integrate to unity.

Comparing with Experiment A detailed study how well the predictions agree with experimental measurements is necessary. For this, the experimental acceptances need to be modeled in detail. The results of the model should be compared to the existing measurements of $\pi^+\pi^-$, K^+K^- , $p\bar{p}$ and pK balance functions. Furthermore, balance functions binned in relative azimuthal angle and by transverse momentum can be compared to experimental results.

Diffusion Constant By simultaneously studying balance functions in relative rapidity and azimuthal separation, it might be possible to distinguish the separation caused by diffusions from the separation caused by string breaking or color-flux tube tunneling at early times.

Freezeout Temperature The exact value of the freezeout temperature was chosen arbitrarily (within a plausible range). A parameter study could explore the relation between the choice of this temperature and the resulting balance functions. The results are expected to be sensitive to any change that alters the final-state yields.

Non-Central Collisions By changing the initial conditions of the hydrodynamics code, centrality as a parameter could be studied. As discussed in the introduction, the balance functions are expected to become broader for increasing impact parameter. The extent of this effect could be tested.

More Lattice QCD Data Currently, lattice quantum chromodynamics data is missing for the ud off-diagonal terms in the charge susceptibility. This data would allow avoiding to interpolate the values of the susceptibility in the region near the critical temperature.

APPENDICES

Appendix A: Notation and Conventions

Units The following units are used:

$$c = \hbar = k_b = 1 \quad (4.1)$$

Special Functions The *Dirac δ -function* is defined by the integral equation

$$\int f(x) \delta(x) dx := f(0) . \quad (4.2)$$

The *Heaviside step function* can be given as

$$\theta(x) := \int_{-\infty}^x \delta(y) dy = \begin{cases} 0 & x < 0 \\ \frac{1}{2} & x = 0 \\ 1 & x > 0 \end{cases} . \quad (4.3)$$

(The value at 0 is an arbitrary convention.)

The *gamma function* is defined as

$$\Gamma(t) := \int_0^{\infty} x^{t-1} e^{-x} dx . \quad (4.4)$$

For $t \in \mathbb{N}$ this simplifies to

$$\Gamma(t) = (n-1)! . \quad (4.5)$$

Minkowski Space 4-vectors are typeset bold, 3-vectors have an arrow:

$$\mathbf{x} = \begin{pmatrix} x^0 \\ x^1 \\ x^2 \\ x^3 \end{pmatrix} \quad \vec{x} = \begin{pmatrix} x^1 \\ x^2 \\ x^3 \end{pmatrix} \quad (4.6)$$

Latin indices are spatial, greek indices can be temporal:

$$i \in \{1, 2, 3\} \quad \mu \in \{0, 1, 2, 3\} \quad (4.7)$$

If a term contains the same index two times, it implies an implicit summation over this index (*Einstein sum convention*).

The Minkowski metric is assumed to be

$$\eta = \begin{pmatrix} 1 & & & \\ & -1 & & \\ & & -1 & \\ & & & -1 \end{pmatrix}. \quad (4.8)$$

Appendix B: Normalization of Maxwell-Jüttner Distribution

We want to calculate the integral

$$d := \int d^3p \exp\left(-\frac{\mathbf{u} \cdot \mathbf{p}}{T}\right). \quad (4.9)$$

d is Lorentz-invariant, so we can choose a reference frame where $\mathbf{u} = (1, 0, 0, 0)$:

$$d = \int p^2 dp d(\cos \theta) d\phi \exp\left(-\frac{E_p}{T}\right) = 4\pi \int_0^\infty p^2 e^{-\frac{E_p}{T}} dp \quad (4.10)$$

Choosing the Lorentz factor as a new variable of integration

$$\gamma := \frac{E_p}{m} = \sqrt{1 + \left(\frac{p}{m}\right)^2} \quad \Leftrightarrow \quad p = m\sqrt{\gamma^2 - 1} \quad (4.11)$$

$$d\gamma = \frac{p}{mE_p} dp \quad \Leftrightarrow \quad dp = \frac{m\gamma}{\sqrt{\gamma^2 - 1}} d\gamma \quad (4.12)$$

gives

$$d = 4\pi m^2 \int_1^\infty m\gamma \sqrt{\gamma^2 - 1} e^{-\frac{m}{T}\gamma} d\gamma. \quad (4.13)$$

Now we can integrate by parts using $\partial_\gamma (\gamma^2 - 1)^{\frac{3}{2}} = 3\gamma \sqrt{\gamma^2 - 1}$:

$$d = 4\pi m^2 \int_1^\infty \frac{m^2}{3T} (\gamma^2 - 1)^{\frac{3}{2}} e^{-\frac{m}{T}\gamma} d\gamma \quad (4.14)$$

$$= 4\pi m^2 \frac{m^2}{3T} \cdot 3 \frac{T^2}{m^2} K_2\left(\frac{m}{T}\right) = 4\pi m^2 T K_2\left(\frac{m}{T}\right), \quad (4.15)$$

giving the normalization.

BIBLIOGRAPHY

BIBLIOGRAPHY

- [1] S. A. Bass, P. Danielewicz, and S. Pratt. “Clocking Hadronization in Relativistic Heavy-Ion Collisions with Balance Functions”. In: *Phys. Rev. Lett.* 85 (13 Sept. 2000), pp. 2689–2692. DOI: 10.1103/PhysRevLett.85.2689.
- [2] S. Pratt, C. Ratti, and W. P. McCormack. “Chemical properties of super-hadronic matter created in relativistic heavy ion collisions”. In: *ArXiv e-prints* (Sept. 2014). arXiv: 1409.2164 [nucl-th].
- [3] D. Drijard et al. “Density, charge and transverse momentum correlations of particles in non-diffractive proton-proton collisions at $\sqrt{s} = 52.5$ GeV”. In: *Nuclear Physics B* 155.2 (1979), pp. 269–294. ISSN: 0550-3213. DOI: [http://dx.doi.org/10.1016/0550-3213\(79\)90269-4](http://dx.doi.org/10.1016/0550-3213(79)90269-4).
- [4] D. Drijard et al. “Quantum number effects in events with a charged particle of large transverse momentum: (II). Charge correlations in jets”. In: *Nuclear Physics B* 166.2 (1980), pp. 233–242. ISSN: 0550-3213. DOI: [http://dx.doi.org/10.1016/0550-3213\(80\)90226-6](http://dx.doi.org/10.1016/0550-3213(80)90226-6).
- [5] H. Aihara et al. “Observation of Strangeness Correlations in e^+e^- Annihilation at $\sqrt{s} = 29$ GeV”. In: *Phys. Rev. Lett.* 53 (23 Dec. 1984), pp. 2199–2202. DOI: 10.1103/PhysRevLett.53.2199.
- [6] J. Adams et al. “Narrowing of the Balance Function with Centrality in Au + Au Collisions at $\sqrt{s_{NN}} = 130$ GeV”. In: *Phys. Rev. Lett.* 90 (17 May 2003), p. 172301. DOI: 10.1103/PhysRevLett.90.172301.
- [7] STAR Collaboration et al. “Longitudinal scaling property of the charge balance function in Au+Au collisions at $s=200$ GeV”. In: *Physics Letters B* 690 (June 2010), pp. 239–244. DOI: 10.1016/j.physletb.2010.05.028. arXiv: 1002.1641 [nucl-ex].
- [8] M. M. Aggarwal et al. “Balance functions from Au+Au, d+Au, and p+p collisions at $s_{NN}=200$ GeV”. In: *Phys. Rev. C* 82.2, 024905 (Aug. 2010), p. 024905. DOI: 10.1103/PhysRevC.82.024905. arXiv: 1005.2307 [nucl-ex].
- [9] G. Westfall and the STAR Collaboration. “Widths of the balance function for charged kaon pairs from Au + Au at $\sqrt{s_{NN}} = 200$ GeV and p + p at $\sqrt{s} = 200$ GeV at RHIC”. In: *Journal of Physics G: Nuclear and Particle Physics* 30.1 (2004), S345. DOI: 10.1088/0954-3899/30/1/040.
- [10] H. Wang. “Study of Particle Ratio Fluctuations and Charge Balance Functions at RHIC”. In: *ArXiv e-prints* (Apr. 2013). arXiv: 1304.2073 [nucl-ex].
- [11] X.-N. Wang and M. Gyulassy. “HIJING: A Monte Carlo model for multiple jet production in pp , pA , and AA collisions”. In: *Phys. Rev. D* 44 (11 Dec. 1991), pp. 3501–3516. DOI: 10.1103/PhysRevD.44.3501. URL: <http://link.aps.org/doi/10.1103/PhysRevD.44.3501>.

- [12] S. A. Bass et al. “Microscopic models for ultrarelativistic heavy ion collisions”. In: *Progress in Particle and Nuclear Physics* 41 (1998), pp. 255–369. DOI: 10.1016/S0146-6410(98)00058-1. eprint: nucl-th/9803035.
- [13] S. Cheng et al. “Statistical and dynamic models of charge balance functions”. In: *Phys. Rev. C* 69.5, 054906 (May 2004), p. 054906. DOI: 10.1103/PhysRevC.69.054906. eprint: nucl-th/0401008.
- [14] C. Alt et al. “System size and centrality dependence of the balance function in $A + A$ collisions at $\sqrt{s_{NN}} = 17.2$ GeV”. In: *Phys. Rev. C* 71 (3 Mar. 2005), p. 034903. DOI: 10.1103/PhysRevC.71.034903.
- [15] A. Bialas. “Balance functions in coalescence model”. In: *Physics Letters B* 579 (Jan. 2004), pp. 31–38. DOI: 10.1016/j.physletb.2003.10.106. eprint: hep-ph/0308245.
- [16] P. Bożek, W. Broniowski, and W. Florkowski. “Balance functions in a thermal model with resonances”. In: *Acta Phys. Hung. A22* (2005), pp. 149–157. DOI: 10.1556/APH.22.2005.1-2.15. arXiv: nucl-th/0310062 [nucl-th].
- [17] P. Bożek. “The balance function in azimuthal angle is a measure of the transverse flow”. In: *Physics Letters B* 609 (Mar. 2005), pp. 247–251. DOI: 10.1016/j.physletb.2005.01.072. eprint: nucl-th/0412076.
- [18] B. Ling, T. Springer, and M. Stephanov. “Hydrodynamics of charge fluctuations and balance functions”. In: *Phys. Rev. C* 89.6, 064901 (June 2014), p. 064901. DOI: 10.1103/PhysRevC.89.064901. arXiv: 1310.6036 [nucl-th].
- [19] G. Agakishiev et al. “Anomalous centrality evolution of two-particle angular correlations from Au-Au collisions at $s_{NN}=62$ and 200 GeV”. In: *Phys. Rev. C* 86.6, 064902 (Dec. 2012), p. 064902. DOI: 10.1103/PhysRevC.86.064902. arXiv: 1109.4380 [nucl-ex].
- [20] S. Pratt and J. Vredevoogd. “Femtoscopia in relativistic heavy ion collisions and its relation to bulk properties of QCD matter”. In: *Phys. Rev. C* 78.5, 054906 (Nov. 2008), p. 054906. DOI: 10.1103/PhysRevC.78.054906. arXiv: 0809.0516 [nucl-th].
- [21] J. D. Bjorken. “Highly relativistic nucleus-nucleus collisions: The central rapidity region”. In: *Phys. Rev. D* 27 (1 Jan. 1983), pp. 140–151. DOI: 10.1103/PhysRevD.27.140.
- [22] S. Pratt. “Accounting for backflow in hydrodynamic-Boltzmann interfaces”. In: *Phys. Rev. C* 89.2, 024910 (Feb. 2014), p. 024910. DOI: 10.1103/PhysRevC.89.024910. arXiv: 1401.0316 [nucl-th].
- [23] F. Cooper and G. Frye. “Single-particle distribution in the hydrodynamic and statistical thermodynamic models of multiparticle production”. In: *Phys. Rev. D* 10 (July 1974), pp. 186–189. DOI: 10.1103/PhysRevD.10.186.
- [24] S. Pratt. “General charge balance functions: A tool for studying the chemical evolution of the quark-gluon plasma”. In: *Phys. Rev. C* 85.1, 014904 (Jan. 2012), p. 014904. DOI: 10.1103/PhysRevC.85.014904. arXiv: 1109.3647 [nucl-th].

- [25] J. Dunkel, P. Talkner, and P. Hänggi. “Relativistic diffusion processes and random walk models”. In: *Phys. Rev. D* 75.4, 043001 (Feb. 2007). DOI: 10.1103/PhysRevD.75.043001. eprint: cond-mat/0608023.
- [26] F. Jüttner. “Das Maxwellsche Gesetz der Geschwindigkeitsverteilung in der Relativtheorie”. In: *Annalen der Physik* 339.5 (1911), pp. 856–882. ISSN: 1521-3889. DOI: 10.1002/andp.19113390503. URL: <http://dx.doi.org/10.1002/andp.19113390503>.
- [27] G. M. Kremer. *Theory and applications of the relativistic Boltzmann equation*. Feb. 2013. URL: http://www.ift.uni.wroc.pl/~karp49/LadekLectures2013/Monday/gmKremer1_49th.pdf.
- [28] E. Weisstein. *Modified Bessel Function of the Second Kind*. May 2014. URL: <http://mathworld.wolfram.com/ModifiedBesselFunctionoftheSecondKind.html>.
- [29] Wolfram Research, Inc. *Mathematica 9.0*. 2012. URL: <http://www.wolfram.com/mathematica/>.
- [30] SymPy Development Team. *SymPy: Python library for symbolic mathematics*. 2014. URL: <http://www.sympy.org>.
- [31] Wikipedia. *Meijer G-function* — *Wikipedia, The Free Encyclopedia*. [Online; accessed 5-June-2014]. 2014. URL: https://en.wikipedia.org/wiki/Meijer_G-function.
- [32] S. Borsányi et al. “Fluctuations of conserved charges at finite temperature from lattice QCD”. In: *Journal of High Energy Physics* 1, 138 (Jan. 2012), p. 138. DOI: 10.1007/JHEP01(2012)138. arXiv: 1112.4416 [hep-lat].
- [33] J. Vredevoogd. “Relativistic Viscous Hydrodynamics for High Energy Heavy Ion Collisions”. In: *ArXiv e-prints* (July 2013). arXiv: 1307.7677 [nucl-th].
- [34] Wikipedia. *Bresenham’s line algorithm* — *Wikipedia, The Free Encyclopedia*. [Online; accessed 23-June-2014]. 2014. URL: https://en.wikipedia.org/wiki/Bresenham's_line_algorithm.
- [35] P. Braun-Munzinger and J. Stachel. “The quest for the quark-gluon plasma”. In: *Nature* 448 (July 2007), pp. 302–309. DOI: 10.1038/nature06080.